High-Field Magnetoresistance of Organic Semiconductors

G. Joshi,[1] M. Y. Teferi,[1] R. Miller,[1] S. Jamali,[1] M. Groesbeck,[1] J. van Tol,[2] R. McLaughlin,[1]
Z. V. Vardeny,[1] J. M. Lupton,[1,3] H. Malissa,[1,*] and C. Boehme[1]

[1]*Department of Physics and Astronomy, University of Utah, Salt Lake City, Utah 84112, USA*
[2]*National High Magnetic Field Laboratory, Florida State University, Tallahassee, Florida 32310, USA*
[3]*Institut für Experimentelle und Angewandte Physik, Universität Regensburg, Universitätsstrasse 31, 93053
Regensburg, Germany*

The magnetoelectronic field effects in organic semiconductors at high magnetic fields are described by field-dependent mixing between singlet and triplet states of weakly bound charge-carrier pairs due to small differences in their Landé g factors that arise from the weak spin-orbit coupling in the material. In this work, we corroborate theoretical models for the high-field magnetoresistance of organic semiconductors, in particular of diodes made of the conducting polymer poly(3,4-ethylenedioxythiophene):poly(styrene-sulfonate) (PEDOT:PSS) at low temperatures, by conducting magnetoresistance measurements along with multifrequency continuous-wave electrically detected magnetic-resonance experiments. The measurements are performed on identical devices under similar conditions in order to independently assess the magnetic-field-dependent spin-mixing mechanism, the so-called Δg mechanism. An understanding of the microscopic origin of magnetoresistance in organic semiconductors is crucial for developing reliable magnetometer devices capable of operating over a broad range of magnetic fields of order 10^{-7}–10 T.

I. INTRODUCTION

The magnetic-field dependencies of electronic and optoelectronic properties of organic semiconductors, such as organic magnetoresistance (OMAR) and organic magnetoelectroluminescence, are frequently attributed to the spin dynamics in the material [1–4]. The observed functionalities in the magnetic-field dependencies are generally explained by the interplay of the hyperfine couplings between the charge-carrier spins and the nuclear spins of the surrounding hydrogen nuclei, which constitute a randomly varying magnetic field. The effects of spin-orbit coupling (SOC) may dominate the magnetoresistance response at high magnetic fields [5]. In addition, at very low temperatures and high fields, thermal spin polarization affects the spin statistics [6]. Whereas the latter effect arises due to incoherent spin-lattice relaxation, the first two processes are coherent in nature. Most organic semiconductors consist of light elements only, and SOC is generally very weak. Nevertheless, at sufficiently high magnetic fields, the minute effects of SOC on the g factors of the charge-carrier pairs, the so-called Δg effect, become apparent [7]. Theoretical models that explain the observed magnetoresistance within the context of the Δg mechanism have been developed [8], but these provide no microscopic insight into the underlying SOC responsible for this spin-mixing

mechanism. These models depend on too many parameters to allow a direct estimation of Δg. To date, merely fitting a magnetoresistance curve does not provide a direct substantiation of the microscopic processes involved.

Magnetoresistive effects of organic semiconductor devices have considerable application potential, since the materials can be easily integrated in a range of different environments. In addition, organic magnetometers potentially function over a very large range of magnetic-field strengths, from tens of tesla down to the submicrotesla regime [9,10]. The employment of magnetoresistive effects in magnetometry applications requires precise knowledge of the functional dependence on the magnetic field and an understanding of the microscopic origins thereof.

Here, we present a high-field magnetoresistance study of organic diodes made of the conducting polymer poly(3,4-ethylenedioxythiophene):poly(styrene-sulfonate) (PEDOT:PSS) with a ratio 1:6 (Clevios P VP AI 4083) [11] at liquid helium-4 temperature as well as an additional independent direct measurement of the charge-carrier g factors from electrically detected magnetic resonance (EDMR) experiments [12] performed on the same devices under similar measurement conditions. This approach provides direct quantitative access to the material parameter Δg, completely independent of the magnetoresistance effects. PEDOT:PSS is an organic conducting material which is technologically relevant due to its high room-temperature conductivity, mechanical

_____

*hans.malissa@utah.edu

flexibility, thermal stability, and processability [13], and is used widely in organic light-emitting diodes. At low temperatures, thin-film diode structures of PEDOT:PSS can show pronounced magnetoresistance effects [14]. In pulsed magnetic resonance experiments, pronounced coherent spin beating can be resolved, providing a clear demonstration that the magnetoconductivity is controlled by pair processes [11]. Even though PEDOT:PSS is a hole conductor, electron injection may still occur in diode structures, enabling charge-carrier pair processes to arise when the holes become localized at low temperatures.

The basic concept of Δg mixing is illustrated in Fig. 1. A charge carrier with a Landé g factor precesses in the presence of an external magnetic field B with a frequency $\omega = g\mu_B B/\hbar$, where μ_B is the Bohr magneton; the case of Larmor precession. In a charge-carrier pair, e.g., an electron-hole pair, where the individual charge carriers experience a small difference of g factors Δg which arises from differences in SOC that the charge-carrier species experience, the precession rates of the two spins will differ. The system will therefore undergo oscillations between singlet $|S\rangle$ and triplet $|T_0\rangle$ with a frequency $\Delta\omega = \Delta g\mu_B B/\hbar$ which scales with Δg (i.e., with the strength of SOC) and the magnitude of B [15,16]. This singlet-triplet oscillation constitutes a field-dependent spin-mixing process. The weakly coupled carrier pairs may either dissociate into free charge carriers and consequently contribute to a current which can be detected in a magnetoresistance experiment or, in materials supporting such species, recombine. The individual spins of the carriers may undergo coherent precession under microwave (MW) irradiation or through incoherent spin-lattice relaxation [17]. Note that this spin-mixing process is basically independent of the charge of the carriers in the pair system
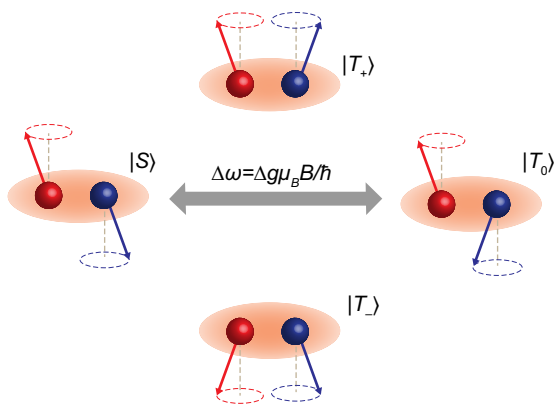
and applies in the same way to unipolar bipolarons as it does to bipolar polaron pairs. The experimental evidence shown here does not allow a distinction to be drawn between these two cases. As discussed in Ref. [11], there is some evidence that, for the given asymmetric injection conditions under which the pronounced low-temperature EDMR is observed, polaron-pair recombination is indeed the dominating spin-dependent process. However, if hole-bipolarons—localized in neighboring PEDOT domains that are separated by PSS domains—were to dominate the observed spin-dependent currents [11], the conclusions drawn from this study would remain unchanged.

Theoretical work by Ehrenfreund *et al.* [8,15,16,18, 19] has provided a consistent description of the magnetic field-effect measurements in the high-field regime above a few hundred millitesla. In particular, Δg mixing between $|S\rangle$ and $|T_0\rangle$ is found to have a pronounced influence on magnetoresistance and other magnetic field effects, such as magnetoelectroluminescence and magneto-photoconductivity. The magnetic field effect generally follows a B dependence in the form of a Lorentzian line $B^2/(B^2 + \Delta B_{1/2}^2)$ with a width $\Delta B_{1/2} = \hbar/2\mu_B\Delta g\tau$ that is inversely proportional to the product of Δg and the lifetime of the charge-carrier pairs τ [15,16]. This model describes the observed magnetoresistance phenomenologically correctly, but the resulting description depends on too many physical parameters. In particular, $\Delta B_{1/2}$ is determined by the product $\Delta g\tau$ even though both the g-factor spread Δg and the decay time τ cannot be estimated independently. Clearly, the magnetoresistance in the high-field regime must originate from the Δg spread as described in the theoretical models [16] but additional, complimentary measurements are needed in order to quantitatively determine Δg.

FIG. 1. Magnetic field-dependent Δg mixing in a carrier-pair system. Charge-carrier pairs can form in any of the four product states, which are $|T_+\rangle$, $|T_-\rangle$, and superpositions of $|S\rangle$ and $|T_0\rangle$. A small but nonzero difference in the charge carriers' g factors leads to differences in their Larmor precession frequencies, and consequently to a field-dependent mixing between $|S\rangle$ and $|T_0\rangle$.

II. EXPERIMENTS AND RESULTS

A convenient way to access the g factors of charge carriers is electron paramagnetic resonance spectroscopy, where the sample is irradiated with MW radiation in the presence of an external magnetic field. At resonance, when the MW frequency matches the Zeeman precession frequency for a field strength of B, spin transitions are driven between the Zeeman-split levels. We employ EDMR spectroscopy [9,12,20–24], where the change in device conductivity is measured under resonant MW excitation. The experimental setup for the detection of these current changes is equivalent to that used for magnetoresistance measurements [24,25], and from the resulting spectra the respective g factors of both charge-carrier species can be determined directly. The spectral shapes and widths of the resonances are governed by the interplay [26] of unresolved hyperfine couplings of the charge-carrier spins to the nuclear spins of the ubiquitous hydrogen nuclei [27] on the one hand, and the small, but nonzero SOC

effects [12,20] on the other. The EDMR line shape at low MW frequencies is predominantly governed by these random hyperfine fields, and differences in g factor are largely obscured by the inhomogeneously broadened lines. The effects of SOC on the g factor and the spectral line shapes are only revealed in EDMR measurements at high MW frequencies, above tens of gigahertz. In recent studies [12,20], we described a method of acquiring EDMR spectra at a range of high frequencies, including the use of a dedicated high-field quasi-optical millimeter-wave spectrometer operating at MW frequencies of 120, 240, and 336 GHz at the National High Magnetic Field Laboratory [28]. These results show that the effects of SOC may lead not only to clearly resolved differences Δg between the g factors of the individual charge carriers in the pair g_1, g_2, but also to g strain broadening [12] and anisotropic g tensors due to the localization of the molecular orbitals in different regions of the polymer [20]. For the particular case of PEDOT:PSS, the relatively high charge-carrier mobilities can give rise to motional narrowing [29] and isotropic effective g tensors, which are accurately described by double-Gaussian line shapes accounting for the inhomogeneous broadening arising from the distributions of the effective g factors in the pair [11,12,29]. Diode structures made from PEDOT:PSS are therefore ideal systems to scrutinize models of magnetoresistance through an independent evaluation of Δg from EDMR measurements.

Figure 2 shows the EDMR spectrum of a device with an ITO/PEDOT:PSS/Al structure at a temperature of 4 K. This dataset is recorded following the procedure reported in Refs. [11] and [12], with a current change measured under a constant-bias voltage of 1.2 V at a resonant MW excitation of 240 GHz [12]. While the individual Gaussian lines appear at almost the same resonance field, a small Δg can be resolved at this high MW frequency from a multifrequency analysis conducted in Ref. [12]. In the limit of completely uncorrelated g factors g_1 and g_2, Δg is given as

$$\Delta g_u = |\langle g_1 \rangle - \langle g_2 \rangle|, \tag{1}$$

i.e., the difference between the center of mass of the individual constituent spectra of both charge carriers in the pair, expressed as g factors. This simple expression, however, does not take into account the correlations between both charge carriers, i.e., the spread of g within each charge-carrier pair. In the limit of fully correlated charge-carrier pairs, Δg is given as

$$\Delta g_c = \langle |g_1 - g_2| \rangle = \frac{\iint |g_1 - g_2| p(g_1) p(g_2) dg_1 dg_2}{\left(\int p(g_1) dg_1 \right) \left(\int p(g_2) dg_2 \right)}, \tag{2}$$

where g_1 and g_2, and the distributions $p(g_1)$ and $p(g_2)$, are given by the individual Gaussian distributions making up the spectrum. We indicate these distributions of g factors
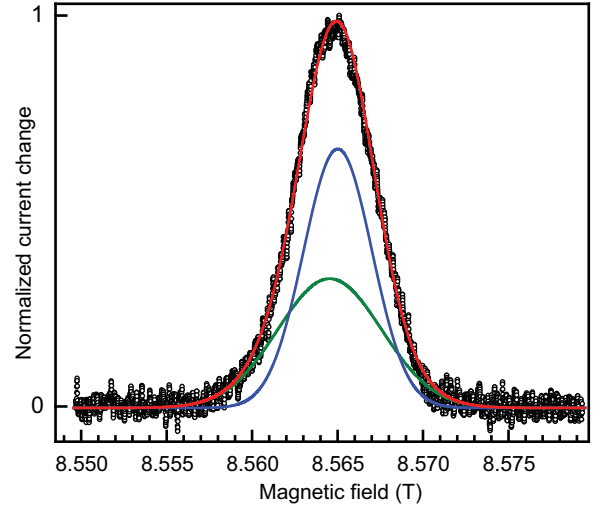

FIG. 2. High-field EDMR spectra measured at a microwave frequency of 240 GHz along with a double-Gaussian line shape (red) obtained by summing the two individual Gaussian lines for the two g values at a given MW frequency. The individual constituents (blue and green) are the calculated Gaussian line shapes for the g factors and g strain values obtained from the multifrequency EDMR measurements as described in Ref. [12], whereas the experimental method is described in Ref. [20].

in Fig. 2. For strongly overlapping resonance lines such as those shown in the figure, the difference between uncorrelated Δg_u and correlated Δg_c can be substantial. We evaluate Δg_u and Δg_c numerically from the measured spectra at different frequencies by performing a global fit using a double-Gaussian line shape [12,26,30] and Eqs. (1) and (2). The results are $\Delta g_u = 1.1 \times 10^{-4}$ and $\Delta g_c = 1.6 \times 10^{-3}$, which differ by more than one order of magnitude.

To relate the spread of g factors to magnetoresistance, we perform low-temperature high-field magnetoresistance measurements over a magnetic field range of up to ± 7 T in a superconducting magnet with an integrated cryostat (Janis SuperOptiMag). Using a SRS SIM928 low-noise voltage source, the PEDOT:PSS diode is biased at approximately 100 μA at constant voltage, and the change in device current is recorded with a low-pass filter setting of 30 Hz of a SR570 current amplifier while sweeping the magnetic field between -7 and 7 T. We sweep the field in both directions in order to minimize the effect of the magnet hysteresis. The measured magnetoconductance response is shown in Fig. 3(a). The steady-state current at $B = 0$ T is 100 μA, and for simplicity, only the field-dependent change from this value is shown on the vertical axis, so that the shifted current value displayed at $B = 0$ T is 0 μA.

III. DISCUSSION

The overall functionality of the magnetocurrent is accurately described as a superposition of three effects.
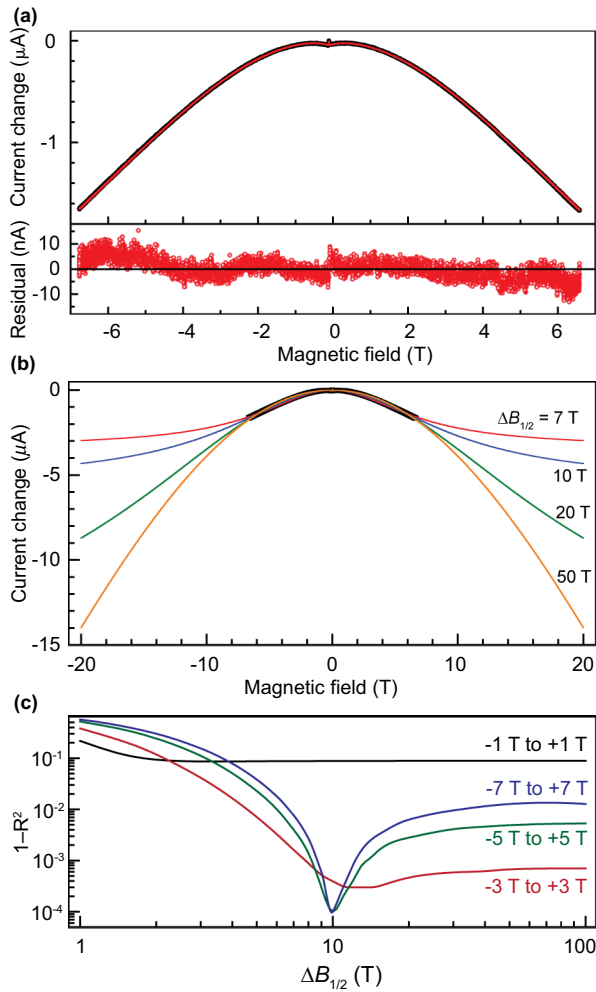
FIG. 3. (a) Upper panel: the magnetoresistance response of a PEDOT:PSS diode at 5 K along with a fit to Eq. 3 (red curve). The vertical offset is adjusted as described in the text. Lower panel: the residuals of the fit. (b) Several fits of Eq. 3 to the experimental data, with the half width at half maximum of the magnetoconductance curve $\Delta B_{1/2}$ set to 7, 10, 20, and 50 T, respectively. All curves fit the measured data well but diverge at higher fields. (c) The coefficient of determination R^2 of the model fit as a function of $\Delta B_{1/2}$. We plot $1 - R^2$ on a logarithmic scale, since $1 - R^2 = 0$ indicates a perfect fit. This procedure is performed for the entire dataset (blue) and for several limited magnetic-field ranges of the experimental magnetoconductance curve shown in (b). (Note that the solid lines in panel (c) serve as guides to the eye only, since $1 - R^2$ is only calculated at discrete values of $\Delta B_{1/2}$.)

For fields exceeding a few hundred millitesla, the Δg-dependent high-field magnetoconductance effect as described above dominates. At lower magnetic fields, below 200 mT, additional ultrasmall and intermediate magnetic field effects are observed [5,10,14,19,31]. These effects are explained in Refs. [5], [19], and [31], and are described by the functionalities $\Delta I \propto B^2/(B^2 + B_0^2)$, which is dominant at fields up to a few millitesla, and $\Delta I \propto$

$B^2/(|B| + B_1)^2$, which occurs up to a few hundred millitesla. The overall magnetocurrent functionality is accurately described over the entire magnetic field range by a phenomenological model taking all three effects into account [31]:

$$\Delta I = A_0 \frac{B^2}{B^2 + B_0^2} + A_1 \frac{B^2}{(|B| + B_1)^2} + A_2 \frac{B^2}{B^2 + \Delta B_{1/2}^2}. \tag{3}$$

In Fig. 3(a), we show a least-squares fit of this model (red curve) to the experimental data. We find best agreement for parameter values $B_0 = 2.64$ mT, $B_1 = 199.5$ mT, and $\Delta B_{1/2} = 10.14$ T. The weighting factors for the individual contributions are $A_0 = -0.042\ \mu$A, $A_1 = 0.05933\ \mu$A, and $A_2 = -5.536\ \mu$A. The fit residuals, i.e., the deviation of the experimental data points from the model, are shown in the lower panel and indicate that the model describes the measured magnetoconductance response accurately. We note that the half width at half maximum of the response, $\Delta B_{1/2}$, established from the model fit, exceeds the magnetic field range accessible in the experiment. The magnetoconductivity does not saturate and so a pronounced baseline of the Lorentzian-like functionality characteristic of the model is not apparent. This absence of a baseline in our magnetoconductance measurement appears to make the quantitative interpretation of the result ambiguous. This problem is illustrated in Fig. 3(b), where the results of partially constrained model fits with fixed $\Delta B_{1/2}$ values as indicated in the labels are compared to the experimental data. The calculated responses differ from each other substantially, but the agreement with the experimental dataset over the measurement range between -7 and $+7$ T is excellent in all cases. From the experimentally accessible magnetic field range, a lower bound for $\Delta B_{1/2}$ of approximately 7 T can be established, but obtaining an estimate for an upper bound does not appear to be possible. Extending the experimentally available magnetic field range may help to establish the baseline of the magnetoconductance response, although we note that currently available dc magnet technology (at highly specialized large-scale laboratories such as the National High Magnetic Field Laboratory in Tallahassee, Florida) is limited to fields below 50 T. From the calculated curves in Fig. 3(b), it is obvious that even this field range may well be insufficient to accurately constrain $\Delta B_{1/2}$ and the baseline of the magnetoconductance response in the case of PEDOT:PSS, since even $\Delta B_{1/2} = 50$ T gives a reasonable description of the measured data.

In order to address this ambiguity, we develop a statistical analysis technique which allows us to determine, for a given experimental magnetoresistance function, whether or not the given finite magnetic field range is sufficient to provide an unambiguous determination of the upper bound of $\Delta B_{1/2}$: First, we calculate the coefficient of

determination R^2 of several model fits as a function of presumed $\Delta B_{1/2}$, which is then no longer a free-fit parameter. The results are shown in Fig. 3(c) (blue trace). For clarity, we plot $1 - R^2$ on a logarithmic scale rather than R^2 itself, since an R^2 value close to unity (i.e., $1 - R^2 = 0$) indicates a perfect fit. A minimum with $1 - R^2 \approx 10^{-4}$ is found close to $\Delta B_{1/2} = 10$ T, in agreement with the least-squares fitting in panel (a), which gave $\Delta B_{1/2} = 10.14$ T; the fit becomes progressively worse for smaller $\Delta B_{1/2}$ values, and exhibits a plateau around $1 - R^2 \approx 10^{-2}$ for larger values. This parametric fitting therefore appears to indicate that a value of $\Delta B_{1/2} \approx 10$ T yields the optimum fit, and that the deviation at larger values is small and possibly insignificant. However, this conclusion could be misleading and a consequence of the choice of the fitting interval. To assess whether the optimum fit for $\Delta B_{1/2} \approx 10$ T is physically meaningful, we decrease the magnetic field range of the experimental data by omitting data points at higher field values and repeat the procedure for each case. The results are shown in Fig. 3(c): the green trace arises from restricting the data points to ± 5 T, with red and black corresponding to ± 3 T and ± 1 T, respectively. The apparent minimum close to 10 T becomes gradually weaker and disappears entirely for the narrowest range of ± 1 T, which indicates that the full dataset does indeed include the onset of a baseline, i.e., the onset of the inflection of the Lorentzian which distinguishes this function in this magnetic field region from a simple parabolic magneto-conductance response. Thus, the pronounced minimum of $1 - R^2 \approx 10^{-4}$ (implying $R^2 \approx 0.9999$) validates the result of the least-squares fit in panel (a) with $\Delta B_{1/2} = 10.14$ T.

The knowledge that $\Delta B_{1/2} = 10.14$ T allows us to establish a value for the product $\Delta g\tau$ of 5.6×10^{-4} ns, although the results of Fig. 3(c) indicate that the uncertainties in this estimate may be substantial. Combined with the values of Δg established above from the EDMR experiments, we estimate τ as 5.1 ns for the extreme case of uncorrelated carrier pairs with Δg_u; and 0.4 ns for a correlated pair with Δg_c. These values serve as upper and lower bounds for τ. Both values are much shorter than the spin-lattice relaxation time T_1 for this material. In Ref. [11], a spin dephasing time $T_2 \approx 300$ ns was established for PEDOT:PSS by means of electrically detected spin-echo measurements [27], which poses an implicit lower bound on T_1. Typically, T_1 is known to be of the order of a few tens of microseconds in organic conductors [32]. The most likely path to reconciling these conflicting observations is that pulsed EDMR and steady-state magnetoresistance probe different carrier-pair ensembles with very different lifetimes. Only the longest-lived most stable pairs interact strongly under resonance and therefore contribute most significantly to the EDMR signal. In contrast, it is the shortest-lived most weakly bound pairs which dominate the nonequilibrium current in magnetoresistance experiments. However, since the effect of SOC in conjugated polymers is purely monomolecular in nature [20], there is no reason not to expect the same Δg in both cases. Our magneto-transport based estimates here of the lifetime of the charge-carrier pair are comparable to the value of < 1 ns given in Ref. [16] for a polythiophene-based blend material for magnetic fields > 0.6 T, which supports intermolecular charge-transfer states. N. b. that the value for the pair lifetime given in Ref. [16] was derived without direct knowledge of Δg.

IV. CONCLUSIONS

In summary, we introduce the technique of high-field EDMR to constrain the parameters for fitting magnetoresistance curves to a phenomenological model. Use of PEDOT:PSS at low temperatures allows us to acquire both magnetoresistance and EDMR data of very high quality, offering maximal constraints on fitting parameters. The metric of the molecular SOC, Δg, is estimated independently from magnetic resonance measurements on identical devices under comparable conditions. The evaluation of the effective width of the magnetoresistance function is complicated by the fact that the measured OMAR response does not saturate over the entire field range investigated, but upper and lower bounds can be established through careful data analysis. The magnetoresistance, together with the Δg distribution obtained from EDMR experiments, reveal that the effective lifetime of charge-carrier pairs in this high-mobility material is surprisingly short and likely in the subnanosecond region. The formulation of a clear understanding of the underlying microscopic physical processes is a key requirement for the development of magnetoresistance-based magnetic-field sensors that work over a very wide range of magnetic fields [10]. Such magnetoresistance-based sensor concepts could supplement magnetic-resonance-based magnetometers, which are limited by hyperfine fields in the limit of low magnetic fields [9], and by the SOC-induced line broadening in the high-field limit [12,20]. The material PEDOT:PSS appears to be particularly versatile in this context: we have previously demonstrated the feasibility of conducting magnetic-resonance-based measurements of the magnetic-field strength on frequency scales spanning almost 12 octaves [12], and magnetoresistive effects can be resolved on field scales down to a few hundred nanotesla [10]. With the systematic magnetoresistive functionality demonstrated here on field scales of up to 7 T, we conclude that PEDOT:PSS-based sensor devices can potentially report on magnetic field scales spanning almost eight orders of magnitude, from 10^{-7} to 10 T.

ACKNOWLEDGMENTS

[1] Ö. Mermer, G. Veeraraghavan, T. L. Francis, Y. Sheng, D. T. Nguyen, M. Wohlgenannt, A. Köhler, M. K. Al-Suti, and M. S. Khan, Large magnetoresistance in nonmagnetic π-conjugated semiconductor thin film devices, Phys. Rev. B **72**, 205202 (2005).

[2] F. J. Wang, H. Bässler, and Z. V. Vardeny, Magnetic Field Effects in π-Conjugated Polymer-Fullerene Blends: Evidence for Multiple Components, Phys. Rev. Lett. **101**, 236805 (2009).

[3] T. D. Nguyen, G. Hukic-Markosian, F. Wang, L. Wojcik, X.-G. Li, E. Ehrenfreund, and Z. V. Vardeny, Isotope effect in spin response of π-conjugated polymer films and devices, Nat. Mater. **9**, 345 (2010).

[4] M. Reufer, M. J. Walter, P. G. Lagoudakis, A. B. Hummel, J. S. Kolb, H. G. Roskos, U. Scherf, and J. M. Lupton, Spin-conserving carrier recombination in conjugated polymers, Nat. Mater. **4**, 340 (2005).

[5] Y. Sheng, T. D. Nguyen, G. Veeraraghaven, O. Mermer, and M. Wohlgenannt, Effect of spin-orbit coupling on magnetoresistance in organic semiconductors, Phys. Rev. B **75**, 035202 (2007).

[6] J. Wang, A. Chepelianskii, F. Gao, and N. C. Greenham, Control of exciton spin statistics through spin polarization in organic optoelectronic devices, Nat. Commun. **3**, 1191 (2012).

[7] J. M. Lupton and C. Boehme, Magnetoresistance in organic semiconductors, Nat. Mater. **7**, 598 (2008).

[8] A. J. Schellekens, W. Wagemans, S. P. Kersten, P. A. Bobbert, and B. Koopmans, Microscopic modeling of magnetic-field effects on charge transport in organic semiconductors, Phys. Rev. B **84**, 075204 (2011).

[9] W. J. Baker, K. Ambal, D. P. Waters, R. Baarda, H. Morishita, K. van Schooten, D. R. McCamey, J. M. Lupton, and C. Boehme, Robust absolute magnetometry with organic thin-film devices, Nat. Commun. **3**, 898 (2012).

[10] P. Klemm, S. Bange, A. Pöllmann, C. Boehme, and J. M. Lupton, Nanotesla magnetoresistance in π-conjugated polymer devices, Phys. Rev. B **95**, 241407(R) (2017).

[11] K. J. van Schooten, D. L. Baird, M. E. Limes, J. M. Lupton, and C. Boehme, Probing long-range carrier-pair spin-spin interactions in a conjugated polymer by detuning of electrically detected spin beating, Nat. Commun. **6**, 6688 (2015).

[12] G. Joshi, M. Y. Teferi, R. Miller, S. Jamali, D. Baird, J. van Tol, H. Malissa, J. M. Lupton, and C. Boehme, Isotropic effective spin-orbit coupling in a conjugated polymer, J. Am. Chem. Soc. **140**, 6758 (2018).

[13] A. Elschner, S.V. Kirchmeyer, W. Lovenich, U. Merker, and K. Reuter, *PEDOT: Principles and Applications of an Intrinsically Conductive Polymer* (CRC Press, Boca Raton, FL, 2010).

[14] P. Klemm, S. Bange, H. Malissa, C. Boehme, and J. M. Lupton, Temperature and current dependence of the magnetoresistive behavior of poly(styrene-sulfonate)-doped poly(3,4-ethylenedioxythiophene) (PEDOT:PSS), J. Photonics Energy **8**, 032216 (2018).

[15] C. Zhang, D. Sun, C.-X. Sheng, Y. X. Zhai, K. Mielczarek, A. Zakhidov, and Z. V. Vardeny, Magnetic field effects in hybrid perovskite devices, Nat. Phys. **11**, 427 (2015).

[16] A. H. Devir-Wolfman, B. Khachatryan, B. R. Gautam, L. Tzabary, A. Keren, N. Tessler, Z. V. Vardeny, and E. Ehrenfreund, Short-lived charge-transfer excitons in organic photovoltaic cells studied by high-field magneto-photocurrent, Nat. Commun. **5**, 4529 (2014).

[17] J. M. Lupton, D. R. McCamey, and C. Boehme, Coherent spin manipulation in molecular semiconductors: Getting a handle on organic spintronics, Chem. Phys. Chem. **11**, 3040 (2010).

[18] E. Ehrenfreund and Z. V. Vardeny, Effects of magnetic field on conductance and electroluminescence in organic devices, Isr. J. Chem. **52**, 552 (2012).

[19] W. Wagemans, P. Janssen, A. J. Schellekens, F. L. Bloom, P. A. Bobbert, and B. Koopmans, The many faces of organic magnetoresistance, SPIN **1**, 93 (2011).

[20] H. Malissa, R. Miller, D. L. Baird, S. Jamali, G. Joshi, M. Bursch, S. Grimme, J. van Tol, J. M. Lupton, and C. Boehme, Revealing weak spin-orbit coupling effects on charge carriers in a π-conjugated polymer, Phys. Rev. B **97**, 161201(R) (2018).

[21] D. R. McCamey, H. A. Seipel, S.-Y. Paik, M. J. Walter, N. J. Borys, J. M. Lupton, and C. Boehme, Spin Rabi flopping in the photocurrent of a polymer light-emitting diode, Nat. Mater. **7**, 723 (2008).

[22] M. Kavand, D. Baird, K. van Schooten, H. Malissa, J. M. Lupton, and C. Boehme, Discrimination between spin-dependent charge transport and spin-dependent recombination in π-conjugated polymers by correlated current and electroluminescence-detected magnetic resonance, Phys. Rev. B **94**, 075209 (2016).

[23] R. Miller, K. J. van Schooten, H. Malissa, G. Joshi, S. Jamali, J. M. Lupton, and C. Boehme, Morphology effects on spin-dependent transport and recombination in polyfluorene thin films, Phys. Rev. B **94**, 214202 (2016).

[24] D. P. Waters, G. Joshi, M. Kavand, M. E. Limes, H. Malissa, P. L. Burn, J. M. Lupton, and C. Boehme, The spin-Dicke effect in OLED magnetoresistance, Nat. Phys. **11**, 910 (2015).

[25] S. Jamali, G. Joshi, H. Malissa, J. M. Lupton, and C. Boehme, Monolithic OLED-microwire devices for ultra-strong magnetic resonant excitation, Nano Lett. **17**, 4648 (2017).

[26] G. Joshi, R. Miller, L. Ogden, M. Kavand, S. Jamali, K. Ambal, S. Venkatesh, D. Schurig, H. Malissa, J. M. Lupton, and C. Boehme, Separating hyperfine from spin-orbit interactions in organic semiconductors by multi-octave magnetic resonance using coplanar waveguide microresonators, Appl. Phys. Lett. **109**, 103303 (2016).

[27] H. Malissa, M. Kavand, D. P. Waters, K. J. van Schooten, P. L. Burn, Z. V. Vardeny, B. Saam, J. M. Lupton, and

C. Boehme, Room-temperature coupling between electrical current and nuclear spins in OLEDs, Science **345**, 1487 (2014).

[28] J. van Tol, L.-C. Brunel, and R. J. Wylde, A quasioptical transient electron spin resonance spectrometer operating at 120 and 240 GHz, Rev. Sci. Instrum. **76**, 074101 (2005).

[29] M. Y. Teferi, J. Ogle, G. Joshi, H. Malissa, S. Jamali, D. L. Baird, J. M. Lupton, L. Whittaker Brooks, and C. Boehme, Tuning effective hyperfine fields in PEDOT:PSS thin films by doping, arXiv:1804.05139 [cond-mat.mes-hall].

[30] S. Stoll and A. Schweiger, EasySpin, a comprehensive software package for spectral simulation and analysis in EPR, J. Magn. Reson. **178**, 42 (2006).

[31] P. Janssen, M. Cox, S. H. W. Wouters, M. Kemerink, M. M. Wienk, and B. Koopmans, Tuning organic magnetoresistance in polymer-fullerene blends by controlling spin reaction pathways, Nat. Commun. **4**, 2286 (2013).

[32] W. J. Baker, T. L. Keevers, J. M. Lupton, D. R. McCamey, and C. Boehme, Slow Hopping and Spin Dephasing of Coulombically Bound Polaron Pairs in an Organic Semiconductor at Room Temperature, Phys. Rev. Lett. **108**, 267601 (2012).